Engineering Structures 56 (2013) 431–442

Contents lists available at SciVerse ScienceDirect

Engineering Structures

journal homepage: www.elsevier.com/locate/engstruct

Seismic performance of steel structures with seesaw energy dissipation system using fluid viscous dampers

Jae-Do Kang [a], Hiroshi Tagawa [b,*]

[a] Graduate School of Environmental Studies, Nagoya University, Nagoya 464-8603, Japan
[b] Graduate School of Engineering, Hiroshima University, Higashi-Hiroshima 739-8527, Japan

ARTICLE INFO

Article history:
Received 3 July 2012
Revised 8 April 2013
Accepted 9 May 2013
Available online 14 June 2013

Keywords:
Passive control
Seesaw mechanism
Earthquake engineering
Energy dissipation
Fluid viscous dampers
Seismic protection

ABSTRACT

This paper presents a new vibration control system based on a seesaw mechanism with fluid viscous dampers. The proposed vibration control system comprises three parts: brace, seesaw, and fluid viscous dampers (FVDs). In this system, only tensile force appears in bracing members. Consequently, the brace buckling problem is negligible. This benefit is useful for steel rods for bracing members. By introducing pre-tension in rods, long steel rods are applicable for bracing between the seesaw members and the moment frame connections over several stories. The relation between the frame displacement and the damper deformation is first derived in consideration of the rod deformation. Simplified analysis models of seesaw energy dissipation system are developed based on this relation. Subsequently, seismic response analyses are conducted for three-story and six-story steel moment frames with and without dampers. In addition to the proposed system, a diagonal-brace-FVD system and a chevron-brace-FVD system are analyzed for comparison. Parameter analyses of rod stiffness and damping coefficient are conducted for the six-story frame. The maximum story drift angle and response of the top floor displacement are discussed. Results show a high capability of seesaw energy dissipation system for improving the structural response.

1. Introduction

For the last few decades, energy dissipation systems have been used increasingly in new and retrofit construction to dissipate earthquake-induced energy into structures [1]. Various energy dissipation systems have been developed such as friction dampers, metallic dampers, viscoelastic dampers, and fluid viscous dampers. Such energy dissipation systems absorb seismic energy and enhance the seismic performance of structures by modifying the dynamic characteristics of a structure [2]. Several references have described the design and implementation of passive control in seismic protection [3–6].

Displacement-dependent passive dampers increase the lateral stiffness of the structure and provide energy dissipation through sliding friction or metallic yielding. During mild or moderate ground motion, however, the seismic energy is not dissipated, although the stiffness increases. Under large ground motions, the seismic performance is improved because of the added energy dissipation and the force-limiting characteristics of the damper [7]. Some researchers have investigated displacement-dependent dampers such as various friction devices [8–11], buckling-restrained braces [12,13], and U-shaped steel dampers [14,15].

The salient benefits of velocity-dependent dampers such as fluid viscous dampers (FVDs) and viscoelastic dampers (VEDs) are energy dissipation for all levels of vibration and flexibility in application. VEDs have been investigated extensively as passive dampers [16–21]. VEDs are comprised of some layers of viscoelastic material bonded with steel plates. The energy input to structures is absorbed through shear deformation of the viscoelastic material. Fluid viscous dampers (FVDs) consist of a cylinder and a stainless steel piston. The cylinder is filled with incompressible silicone fluid that has stable properties over a wide range of operating temperatures. Dampers are activated by the transfer, through small orifices, of silicone fluids between chambers at opposite ends of the unit [22]. FVDs can also be used in innovative configurations that amplify the velocity across the device, including toggle brace systems, scissor–jack systems, amplifying brace systems, and lever arm systems [1,23–25].

This study investigates passive vibration control system based on a seesaw mechanism using fluid viscous dampers (FVDs). In the proposed seesaw energy dissipation system (SEDS), only tension force is generated in bracing members. The brace buckling need not be considered. This paper first presents the relation between the frame displacement and the damper deformation obtained by considering the rod deformation. Based on this relation, simplified analysis models of seesaw energy dissipation system have been developed. Then, seismic response analyses are

* Corresponding author. Tel./fax: +81 82 424 7799.
E-mail address: htagawa@hiroshima-u.ac.jp (H. Tagawa).

0141-0296/$ - see front matter © 2013 Elsevier Ltd. All rights reserved.
http://dx.doi.org/10.1016/j.engstruct.2013.05.015

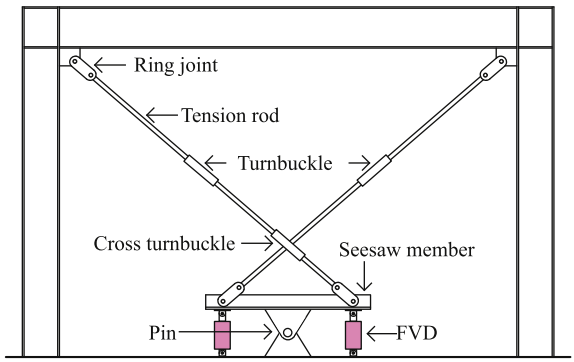

Fig. 1. Proposed vibration control system.

conducted for three-story and six-story steel moment frames with and without dampers. In addition to the proposed system, the diagonal-brace-FVD system and the chevron-brace-FVD system are analyzed for comparison. Parameter analyses of rod stiffness and damping coefficient are conducted for the six-story frame. The maximum story drift angle, response of top floor displacement, base shear force, and peak acceleration are discussed. Results demonstrate the capability of seesaw energy dissipation system for improving structural response effectively.

2. Seesaw energy dissipation system (SEDS)

2.1. Fluid viscous dampers

Fluid viscous dampers (FVDs) include a piston head with orifices contained in a damper-housing filled with fluid, which is mostly a compound of silicone or a similar type of oil. Energy is dissipated in the damper as the piston rod moves through the fluid and forces the fluid to flow through the orifices in the piston head [26]. The force F_D in a FVD is calculated as

$$F_D = Cv^{\vartheta}, \tag{1}$$

where F_D denotes the damper force, C represents the damping coefficient, v stands for the relative velocity between the ends of the damper, and ϑ signifies an exponent that controls the shape of the force velocity relation. The typical values of ϑ are between 0.5 and 2.0. FVDs with $\vartheta > 1$ are generally not used in seismic design applications. Those with $\vartheta < 1$ are called nonlinear FVDs [27]. For high-velocity applications, nonlinear FVDs are used to avoid exceeding the device force capacity. In these nonlinear FVDs, the force is a fractional power law of the velocity [28]. Those with $\vartheta = 1$ are called linear FVDs, in which the damper force is proportional to the relative velocity. This study adopts linear FVDs.

2.2. Seesaw-brace systems

Kang and Tagawa proposed a vibration control system with long rods and seesaw mechanism [29,30]. Fig. 1 portrays the proposed vibration control system comprising a Brace, Seesaw, and FVDs. A couple of FVDs are installed in the seesaw member, which is pin-supported. The brace members comprise two tension rods, turnbuckles, and a cross-turnbuckle. Tension rods intersect from the edge of the seesaw member. By introducing pre-tension in rods, only tensile force appears in bracing members. Accordingly, the brace buckling problem is negligible, and steel rods are applicable as bracing between the seesaw member and the moment frame connections over some stories. When the frame deforms under a lateral load, the FVDs dissipate energy via movement of the piston through a highly viscous fluid. When the lateral load direction reverses, tensile axial force is generated immediately in the opposite rod. This behavior is based on the seesaw mechanism characteristics.

One benefit of this system is that it enables the long steel rods to be used as bracing between the seesaw member and the moment frame connections over some stories, as shown in Fig. 8d. Accordingly, one damping device mounted on ground level can control the frame vibration instead of mounting the damping device on every floor level. This advantage has been confirmed using an analytical approach [29,30].

3. Formulation of SEDS

3.1. Damper deformation

To consider rod deformation as shown in Fig. 2, the horizontal displacement δ of the frame is expressed as

$$\delta = \delta_r + \delta_b, \tag{2}$$

where δ_r signifies the horizontal displacement of the frame attributable to damper deformation, and where δ_b stands for the horizontal displacement of the frame attributable to rod deformation.

The relation between the damper deformation (δ_D) and horizontal displacement (δ) of the frame has been obtained as [30]

$$\delta_D = \left(1 - \frac{\xi}{\cos\alpha}\right)\frac{\cos\alpha\cos\beta}{\sin(\alpha+\beta)}\delta, \tag{3}$$

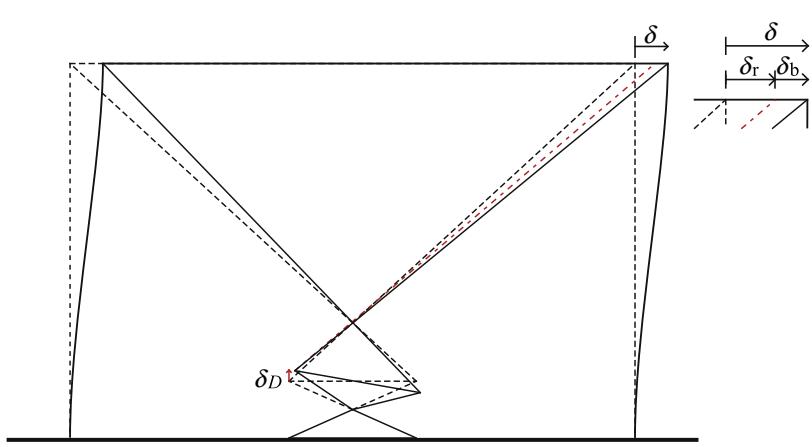

Fig. 2. Analysis of SEDS movement.

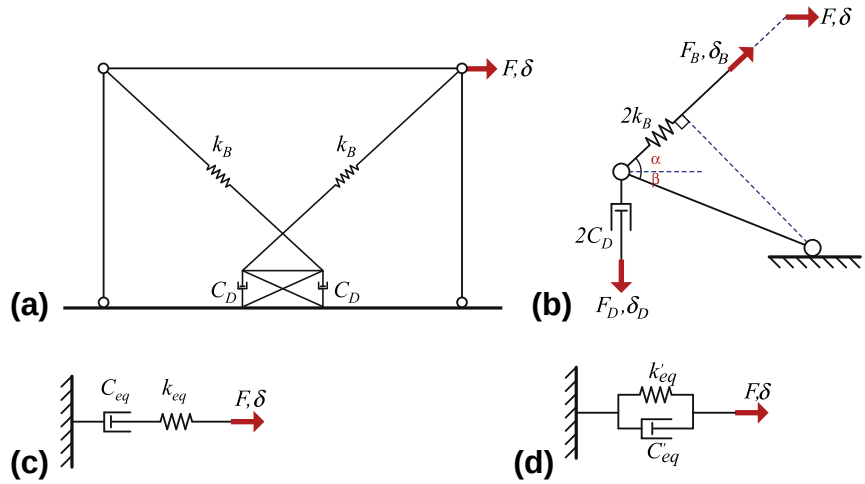

Fig. 3. Analysis of forces acting on a frame with FVDs: (a) exact model, (b) simple model, (c) equivalent Maxwell model, and (d) generalized Kelvin model.

Table 1
Properties of the SDOF structure with SEDS.

	Property	Value
Frame	Width	6000 mm
	Height	4000 mm
	Mass	100 ton
	Natural period	0.359 s
Exact model	Width of seesaw	1600 mm
	Height of seesaw	580 mm
	Rod stiffness	35 kN/mm
	Damping coefficient of FVDs	5 kNs/mm
Equivalent Maxwell model	Rod stiffness	38.67 kN/mm
	Damping coefficient of FVDs	6.27 kNs/mm
Generalized Kelvin model	Rod stiffness	34.40 kN/mm
	Damping coefficient of FVDs	0.7 kNs/mm

where α represents the horizontal angles of brace, and β denotes the angle between the connection member and center pin, and where ξ signifies the rod deformation factor.

Constantinou et al. [1] discussed the relation between the story displacement of frame and damper displacement using a magnification factor of

$$\delta_D = f\delta, \tag{4}$$

where f represents the magnification factor: $f = 1.0$ for the chevron brace system and $f = \cos\theta$ for the diagonal brace system where θ is the angle of brace inclination. The toggle–brace system can give a value of f larger than unity.

When the brace is assumed to be rigid, considering Eq. (3), the magnification factor of the SEDS is expressed simply as

$$f_R = \frac{\cos\alpha\cos\beta}{\sin(\alpha+\beta)}. \tag{5}$$

Eqs. (3) and (5) give the relation of $\delta_r = \delta_D/f_R$. Furthermore, $\delta_b = \delta_B/\cos\alpha$, where δB = rod deformation. Accordingly, considering Eq. (2), the damper deformation is expressed as

$$\delta_D = f_R\delta - \frac{f_R}{\cos\alpha}\delta_B. \tag{6}$$

Eq. (6) shows that the damper deformation decreases as the rod deformation increases.

The magnification factor of the seesaw system, which is related to the damping effect, has been discussed with numerical analysis results [30].

3.2. Simplified analysis model of SEDS

To analyze the proposed system as a simplified single-degree-of-freedom (SDOF) system with SEDS using FVDs, the horizontal stiffness and damping coefficient of a SEDS are needed. The SEDS can be described mathematically as a series of the spring–dashpot model, i.e. the Maxwell model, as presented in Fig. 3c. Displacements of the left and right damper can be assumed as equal if the seesaw member is sufficiently stiff. Furthermore, the rod axial force is assumed to maintain tension by introducing a proper

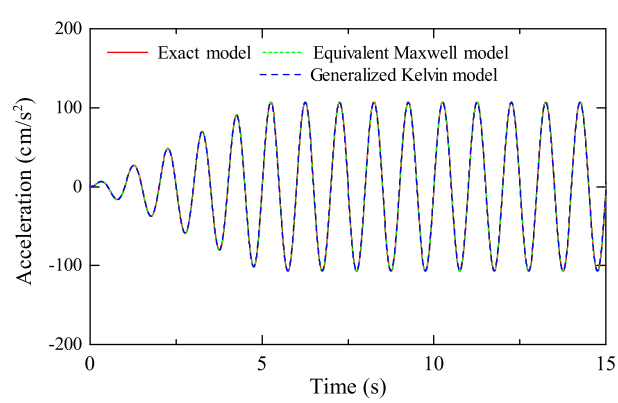

Fig. 4. Time–history response of acceleration at the top floor of a single–story structure.

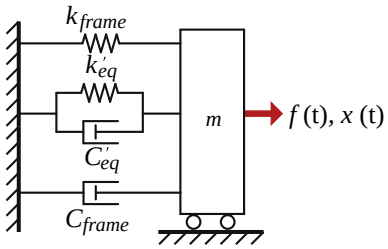

Fig. 5. Equivalent model of a single-story structure with SEDS.

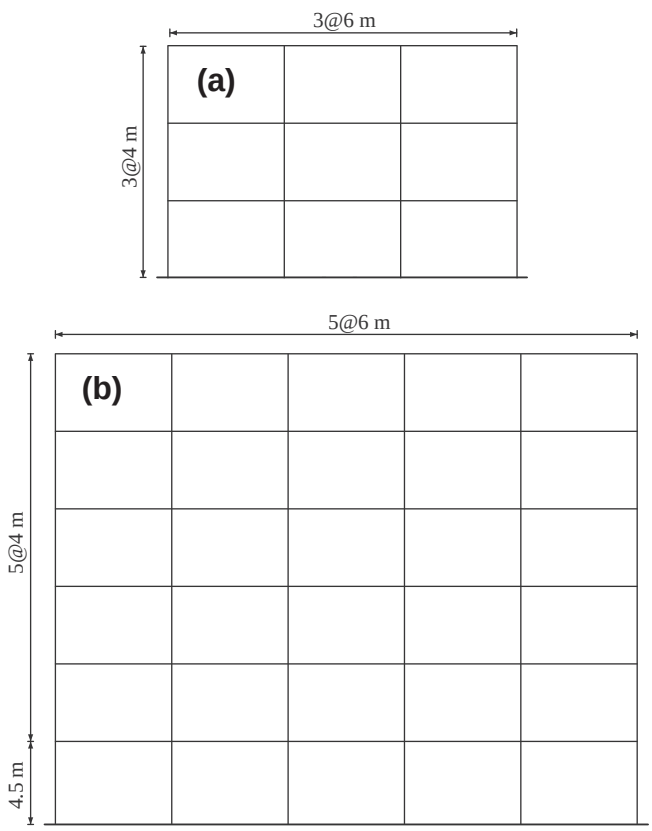

Fig. 6. Steel moment frame (bare frame): (a) three-story and (b) six-story.

amount of pre-tension force. In this case, the exact model presented in Fig. 3a can be modeled using the simple model depicted in Fig. 3b. Considering the moment equilibrium around the seesaw pin, the following relation is obtained.

$$F_B = \frac{\cos\beta}{\sin(\alpha+\beta)} F_D \tag{7}$$

Therein, F_B is the rod force and F_D is the damper force, which are obtained respectively as

$$F_B = 2k_B\delta_B, \quad F_D = 2C_D\dot{\delta}_D, \tag{8a, b}$$

where k_B denotes the rod stiffness and C_D denotes the damper coefficient. The relation between the external horizontal force F and axial force F_B in the rod is

$$F = F_B \cos\alpha. \tag{9}$$

From Eqs. (6), (7), (8), and (9), the following relation is obtained.

$$\dot{\delta} = \frac{F}{2C_D f_R^2} + \frac{\dot{F}}{2k_B\cos\alpha^2} \tag{10}$$

Eq. (10) is the governing equation of the Maxwell model, as depicted in Fig. 3c. The equivalent rod stiffness k_{eq} and damping coefficient C_{eq} from Eq. (11) is definable as

$$k_{eq} = 2k_B\cos\alpha^2, \quad C_{eq} = 2C_D f_R^2. \tag{11a, b}$$

To verify the equivalent rod stiffness and damping coefficient, the dynamic response analysis was conducted. A nonlinear dynamic analysis program: SNAP ver. 5 [31] was used for the dynamic response analysis in this study. Table 1 presents properties of the system used in the analysis. The frame response to the sine wave excitation with a frequency $\omega = 6.28$ rad/s was analyzed. Fig. 4 shows the time–history response of acceleration for the exact and simplified models with dampers. This figure shows that the response of the equivalent Maxwell model agrees well with that of the exact model.

For further simplification, the Kelvin model is considered, as presented in Fig. 3d. In this model, the external force is expressed as

$$F = k'_{eq}\delta + C'_{eq}\dot{\delta}, \tag{12}$$

where k'_{eq} and C'_{eq} respectively represent the generalized system stiffness and the generalized damping coefficient. Based on the complex damping theory [32], they are definable as

$$k'_{eq} = \frac{(k_{eq})(\omega C_{eq})^2}{(k_{eq})^2 + (\omega C_{eq})^2}, \quad C'_{eq} = \frac{(k_{eq})^2(C_{eq})}{(k_{eq})^2 + (\omega C_{eq})^2}, \tag{13}$$

where ω is the frequency of the original structure. Fig. 4 shows that the response of the generalized Kelvin model also agrees well with that of the exact model. The equation of motion for the equivalent system, as presented in Fig. 5 is written as

$$m\ddot{x} + \left(C_{frame} + C'_{eq}\right)\dot{x} + \left(k_{frame} + k'_{eq}\right)x = f(t), \tag{14}$$

where m denotes the mass, k_{frame} and C_{frame} respectively represent the stiffness and the damping coefficient of the frame, and $f(t)$ signifies the external dynamic load.

4. Seismic responses of steel frames with SEDS

4.1. Design of the moment frame

A steel moment frame was designed to meet current Japan seismic code requirements for both strength and drift. Fig. 6a shows the steel moment frame without dampers, which consists of three bays and three stories. The steel sections of H-350 × 350 × 12 × 19 for columns and H-450 × 200 × 9 × 14 for beams are used. The yield strength of the steel material is assumed as 235 N/mm^2. The mass of each story is set as 70 tons. The story shear coefficient in the first story at the final stage of the nonlinear static pushover analysis was obtained as the base shear coefficient (CB) = 0.554. The eigenvalue analysis provided the fundamental natural period as 0.758 s. Fig. 6b shows the steel moment frame without dampers, which consists of five bays and six stories. The steel sections of H-400 × 400 × 18 × 28 for all columns, 600 × 200 × 10 × 15 for beams at 2F–5F, and H-500 × 200 × 10 × 16 for beams at the 6th and top floor are used, and the yield strength of the steel material is assumed to be 325 N/mm^2. The mass of each story is set as 130 tons. The story shear coefficient in the first story at the final stage of the nonlinear static pushover analysis was obtained as the base shear coefficient (CB) = 0.378. Eigenvalue analysis provided the fundamental natural period as 1.23 s. Stiffness-proportional damping is considered with a 2% damping ratio for the first mode throughout this paper.

Table 2
Seismic ground motions used for analysis.

Earthquakes (label)	Year	Peak ground velocity (PGV) (cm/s)	Peak ground acceleration (PGA) (cm/s^2)	Duration (s)
El Centro NS (ELC)	1940	50	510.8	30
Taft EW (TAF)	1952	50	496.9	30
Hachinohe NS (HAC)	1968	50	329.9	30
Kobe NS (KOB)	1995	50	499.9	30

Table 3
Analysis parameters.

Story	Element	f_c (kN m)	f_y (kN m)	γ_1	γ_2	Hysteresis loops
Three-story	Beam	383.13	387.00	0.99	0.01	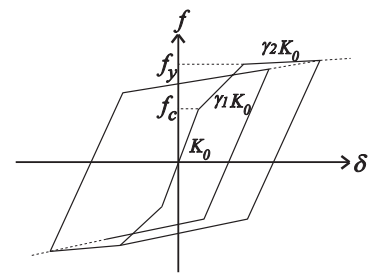
	Column	586.08	592.00	0.99	0.01	
Six-story	Beam	685.33	692.25	0.99	0.01	
	Column	1618.40	1634.75	0.99	0.01	

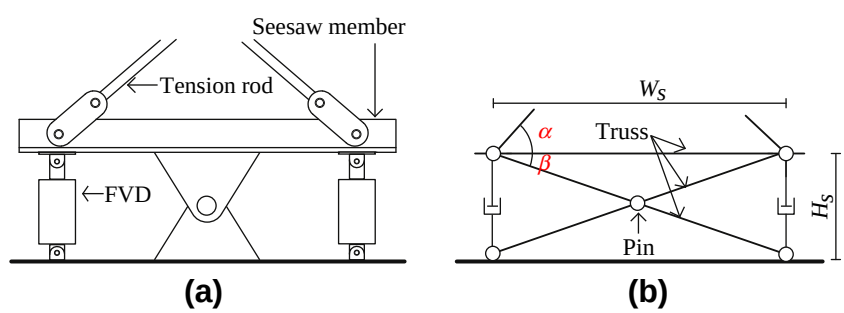

Fig. 7. Modeling of SEDS: (a) details of SEDS and (b) analysis model.

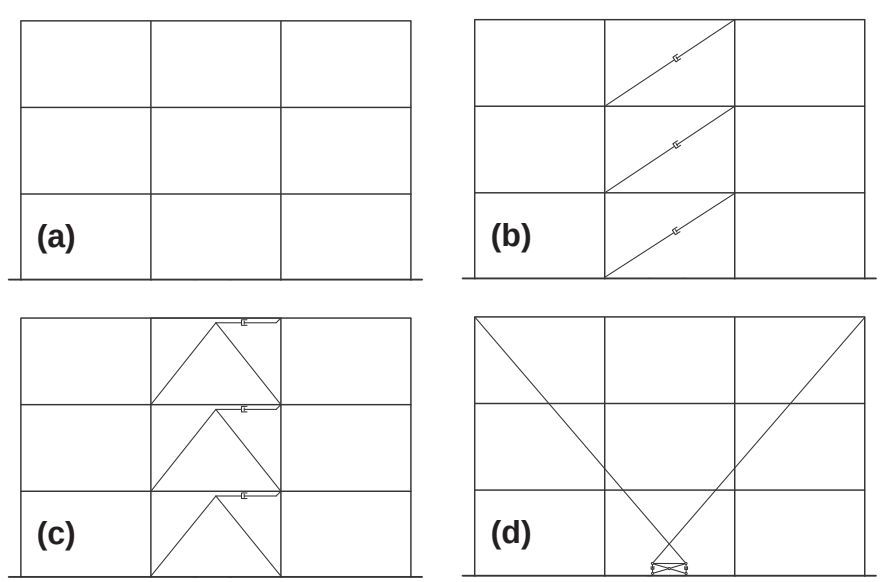

Fig. 8. Analysis models with dampers: (a) bare frame, (b) Model DG, and (c) Model CV, and (d) Model SS.

Table 4
Analysis parameters.

Story	Model	k_B (kN)	C_D (kN s/mm)	N	W_s (mm)	H_s (mm)	α (°)	β (°)
Three-story	DG	∞	1	3	–	–	–	–
	CV	∞	1	3	–	–	–	–
	SS	26.75	1	2	1600	580	49.37	19.93
Six-story	DG	∞	2	6	–	–	–	–
	CV	∞	2	6	–	–	–	–
	SS	35	2	2	4000	1000	54.11	14.07

k_B = rod stiffness, C_D = damping coefficient, N = number of dampers, W_s = width of seesaw, H_s = height of seesaw.

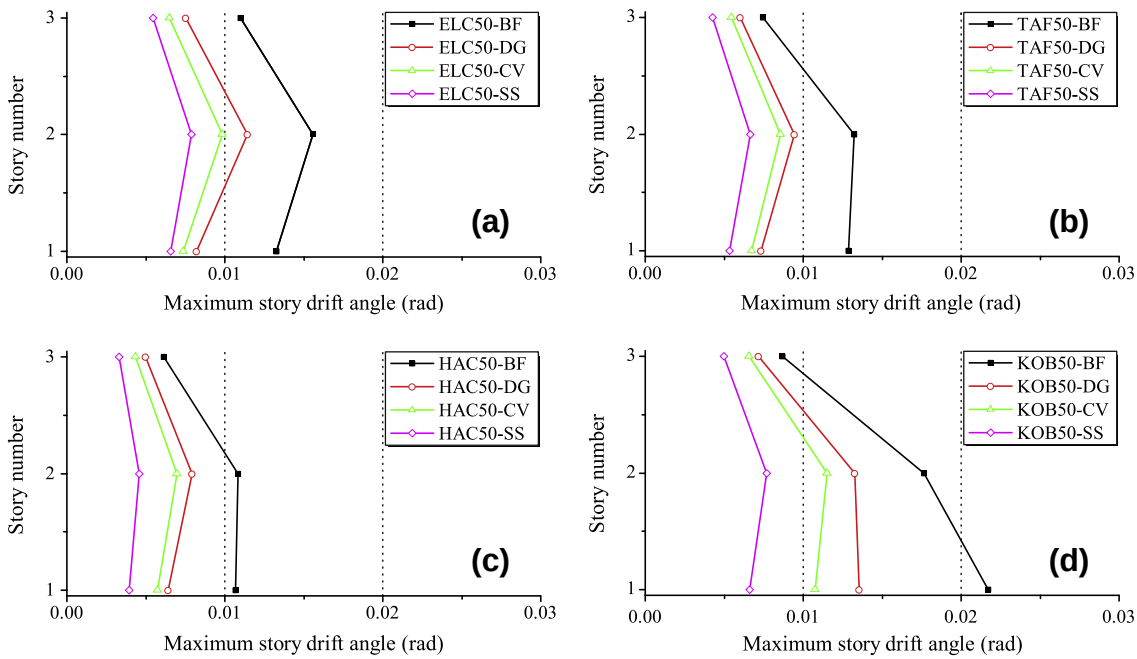

Fig. 9. Maximum story drift angle distribution: (a) El Centro 1940 NS, (b) Taft 1952 EW, (c) Hachinohe 1968 NS, and (d) Kobe 1995 NS.

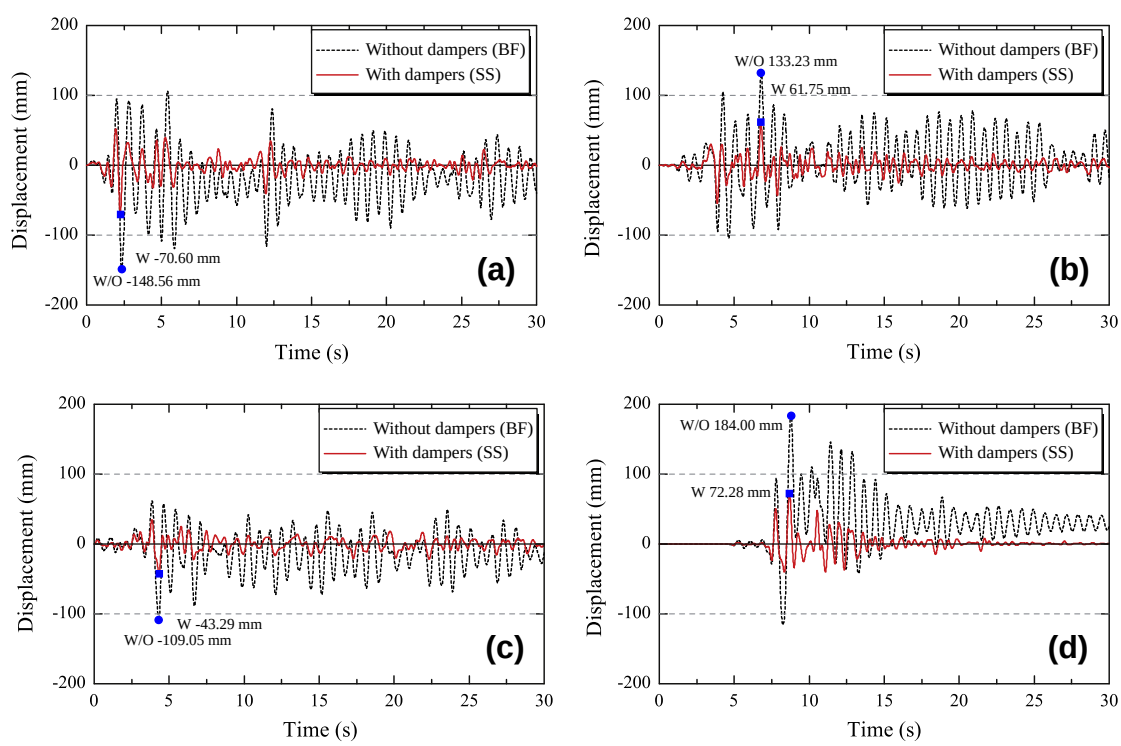

Fig. 10. Time–history response of displacement at the top floor of Model BF and SS: (a) El Centro 1940 NS, (b) Taft 1952 EW, (c) Hachinohe 1968 NS, and (d) Kobe 1995 NS.

Table 5
Maximum displacement of the top floor of three-story structures.

Input motion	Model	Without device (mm)	With device (mm)	Ratio
El Centro	DG	148.59	108.46	0.73
	CV		93.71	0.63
	SS		70.60	0.48
Taft	DG	133.20	90.75	0.68
	CV		81.89	0.61
	SS		61.75	0.46
Hachinohe	DG	109.05	76.02	0.70
	CV		67.12	0.62
	SS		43.29	0.40
Kobe	DG	183.88	135.66	0.74
	CV		115.26	0.63
	SS		72.28	0.39

Table 6
Properties of the three-story structure with SEDS.

Property	Value
Exact model	
Width of seesaw	1600 mm
Height of seesaw	580 mm
Rod stiffness	26.75 kN/mm
Damping coefficient of FVDs	1 kN s/mm
Equivalent Maxwell model	
Rod stiffness	22.69 kN/mm
Damping coefficient of FVDs	0.86 kN s/mm
Generalized Kelvin model	
Rod stiffness	2.03 kN/mm
Damping coefficient of FVDs	0.78 kN s/mm

4.2. Earthquake ground motions

Four earthquake records were used as input ground motions: the 1940 El Centro earthquake record, the 1952 Taft earthquake record, the 1968 Hachinohe earthquake record, and the 1995 Japan Meteorological Agency (JMA) Kobe record. Seismic duration of 30 s was considered for all motions. These records used in the analysis were scaled so that the peak ground velocity was equal to 50 cm/s (Level 2). According to the Japanese seismic design standards for high-rise buildings, Level 2 corresponds to severe earthquakes of the maximum class that might occur in the future. The safety criterion at this level is that, although parts of the

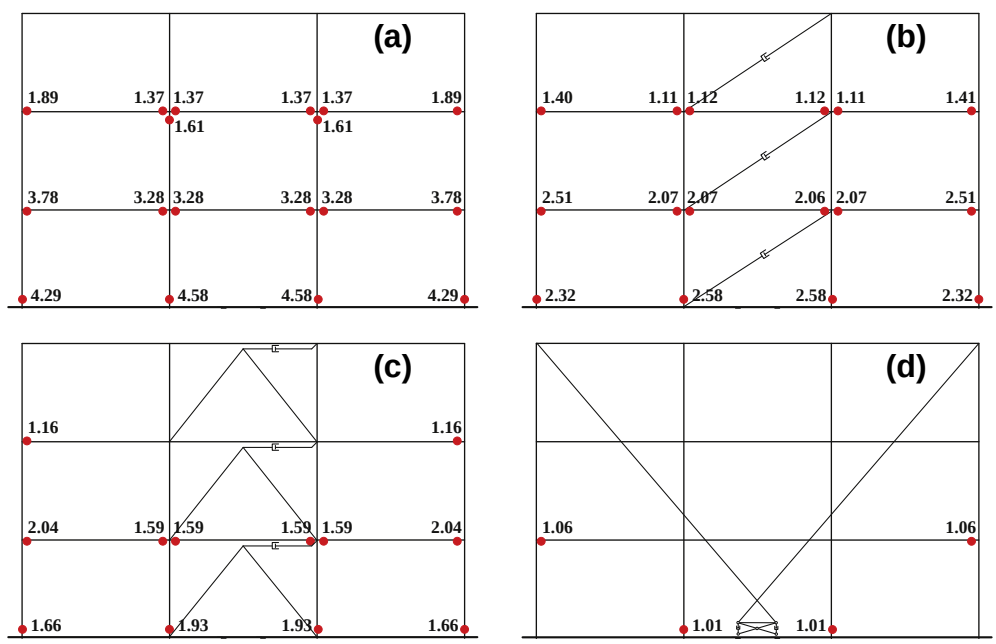

Fig. 11. Plastic hinge formation under the Kobe earthquake: (a) bare frame, (b) Model DG, (c) Model CV, and (d) Model SS.

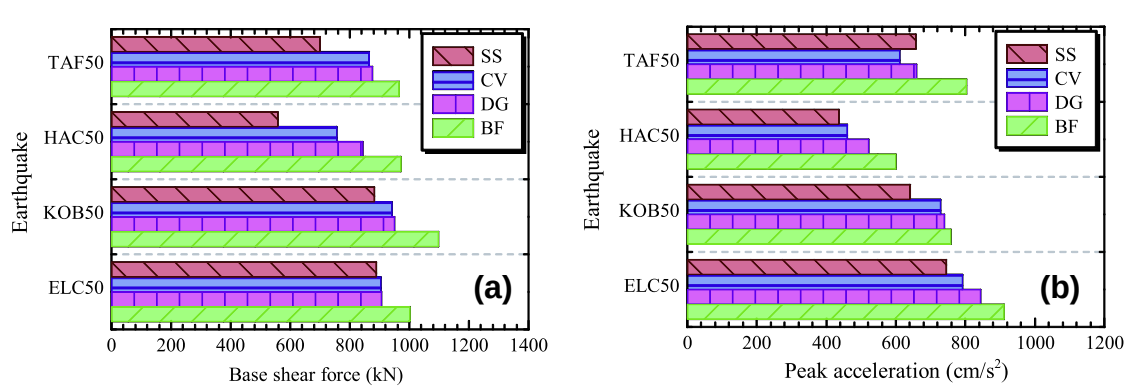

Fig. 12. Base shear force and peak acceleration of three-story structures.

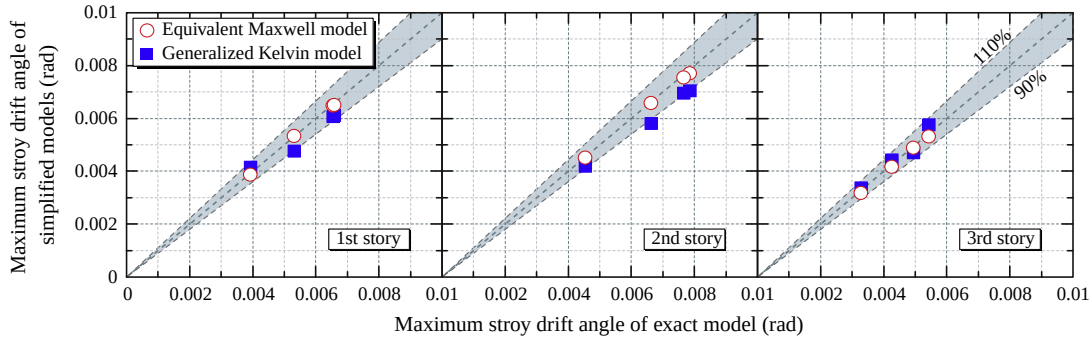

Fig. 13. Maximum story drift angles of three-story structures with exact model and simplified models of SEDS.

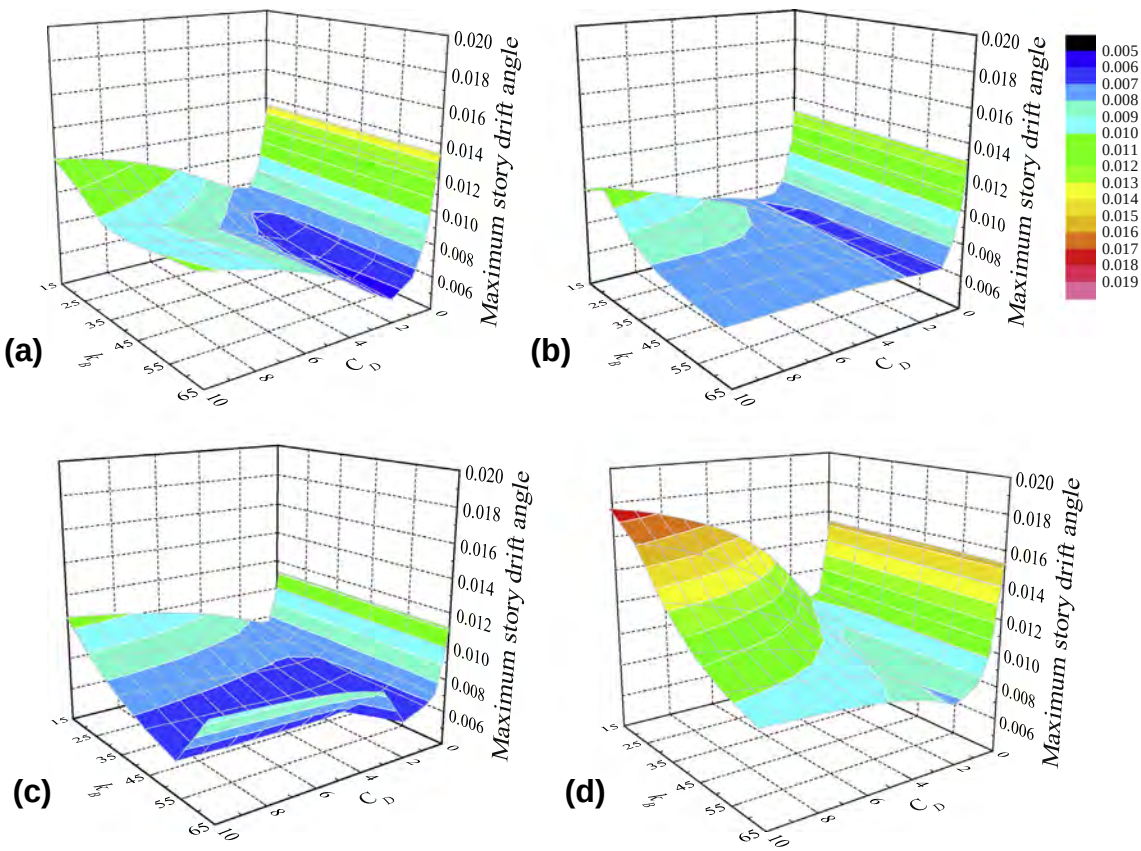

Fig. 14. Variations of maximum story drift angle by rod stiffness and damping coefficient: (a) El Centro 1940 NS, (b) Taft 1952 EW, (c) Hachinohe 1968 NS, and (d) Kobe 1995 NS.

frame might enter the plastic region, excessively large deformation must be prevented. Table 2 shows the peak ground velocity (PGV) and peak ground acceleration (PGA) of the scaled motions.

4.3. Description of analysis models

The beams and columns were modeled using the beam element with plastic hinges at the member ends. The plastic moments at column and beam ends are presented in Table 3. Fig. 7a portrays the SEDS detail, which consists of FVDs, tension rods, and a pin-supported seesaw member. Fig. 7b shows the analysis model, in which some rigid truss members form both the seesaw member and the pin-support. The FVDs are modeled by the dashpot element. The rods are modeled using the elastic spring element.

Analysis models of four types are considered. One is the bare frame (BF) without dampers, as described in Section 4.1. Others are frames with dampers, as presented in Fig. 8. The frames with the diagonal brace system (DG) and chevron brace system (CV) are equipped with linear FVDs attached with the rigid brace. For models DG and CV, damping devices are installed at all stories. In contrast, the frame with proposed system (SS) has one damping device on the ground level. Tension rods are connected to the top floor at the outside bay. Table 4 presents analysis parameters. To examine the effects of the damper installation method, the damping coefficient is set as the same value: $C_D = 1$ kN s/mm for the three-story structure and $C_D = 2$ kN s/mm for the six-story structure. The rods were modeled using the elastic spring element considering the high tensile strength steel as the material.

4.4. Seismic responses of the three-story structure

4.4.1. Maximum story drift angle

Fig. 9 depicts the maximum story drift angle distributions. The maximum story drift angles in Model SS are smaller than 0.01 rad

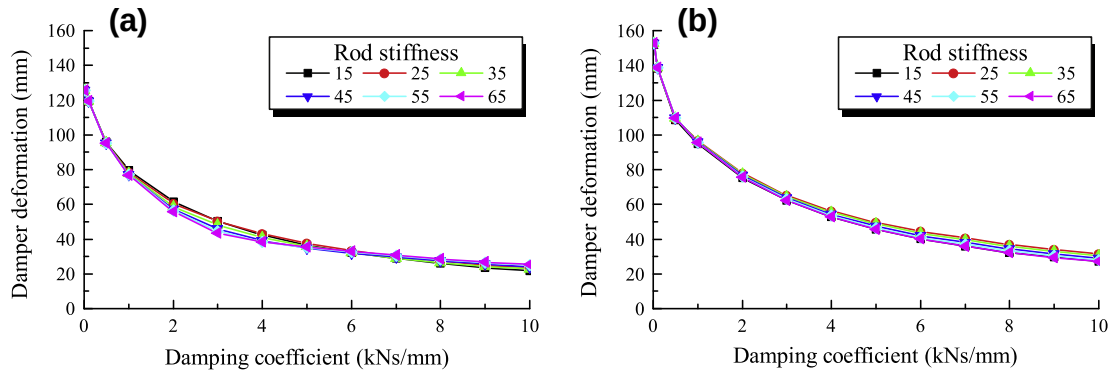

Fig. 15. Effects of rod stiffness and damping coefficient on the damper deformation: (a) El Centro 1940 NS and (b) Kobe 1995 NS.

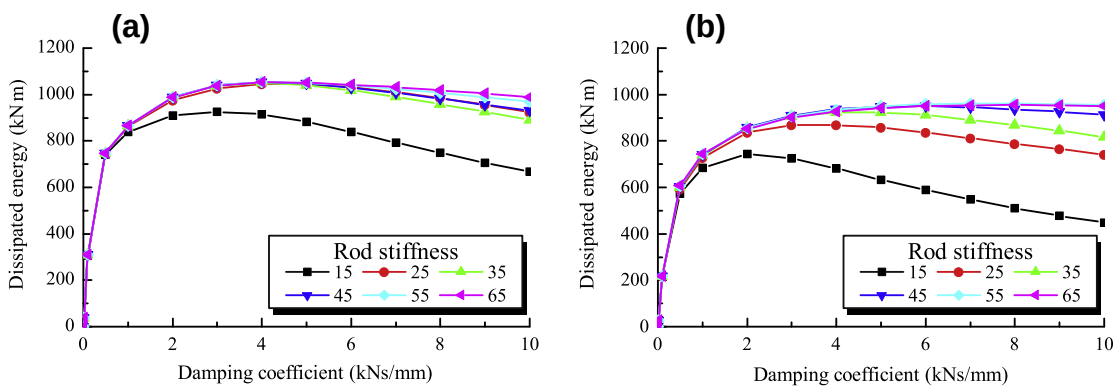

Fig. 16. Effects of rod stiffness and damping coefficient on dissipated energy of FVDs: (a) El Centro 1940 NS and (b) Kobe 1995 NS.

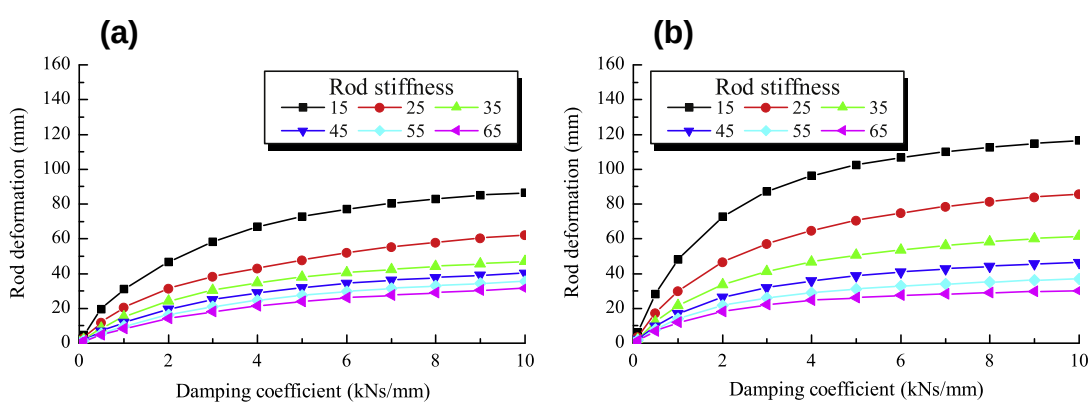

Fig. 17. Effects of rod stiffness and damping coefficient on rod deformation: (a) El Centro 1940 NS and (b) Kobe 1995 NS.

for all earthquakes. The peak of maximum story drift angles for Model DG are reduced by 17–38%. Those for Model CV are reduced by 35–47%. Those for Model SS are reduced by 49–65%. Moreover, the maximum story drift angle at the first floor of Model SS for Kobe earthquake is reduced about 70%. The reduction ratios of the story drift angles demonstrate the effectiveness of the SEDS in addition to requiring fewer dampers than other systems.

4.4.2. Time–history responses of displacement

Fig. 10 shows the respective time–history responses of displacement at the top floors of Models BF and SS. These figures reveal that the proposed system reduces the response displacement effectively. For the Kobe earthquake, the proposed system reduced the residual displacement observed at the final stage of analysis. Table 5 presents the maximum displacement of the top floor and the ratio of the value of the models with dampers to that of the model without dampers (BF).

4.4.3. Plastic hinge formation

Fig. 11 portrays the location of plastic hinges and shows their yield ratio at the final stage of seismic response analysis for Kobe earthquake. In the bare frame, the plastic hinges form at all beam-ends except for the top beams, and at the column-base in the first story. For Model DG, the number of forming plastic hinges did not decrease. For Model SS, however, both the number of plastic hinges and their yield ratios decreased.

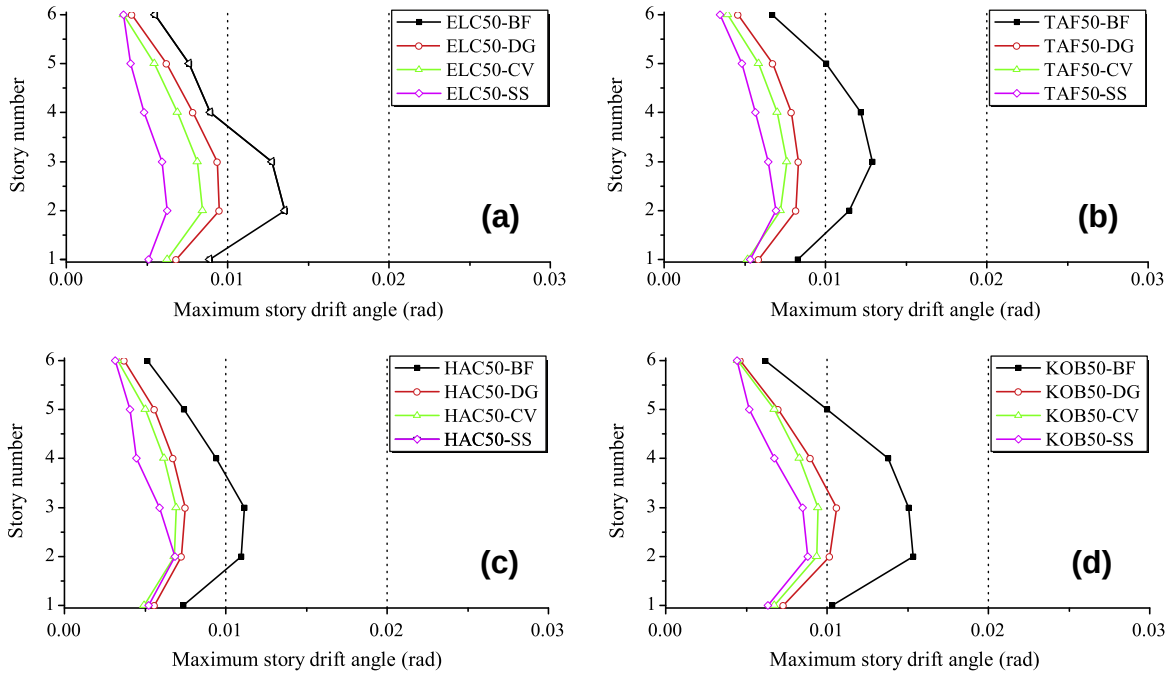

Fig. 18. Maximum story drift angle distribution: (a) El Centro 1940 NS, (b) Taft 1952 EW, (c) Hachinohe 1968 NS, and (d) Kobe 1995 NS.

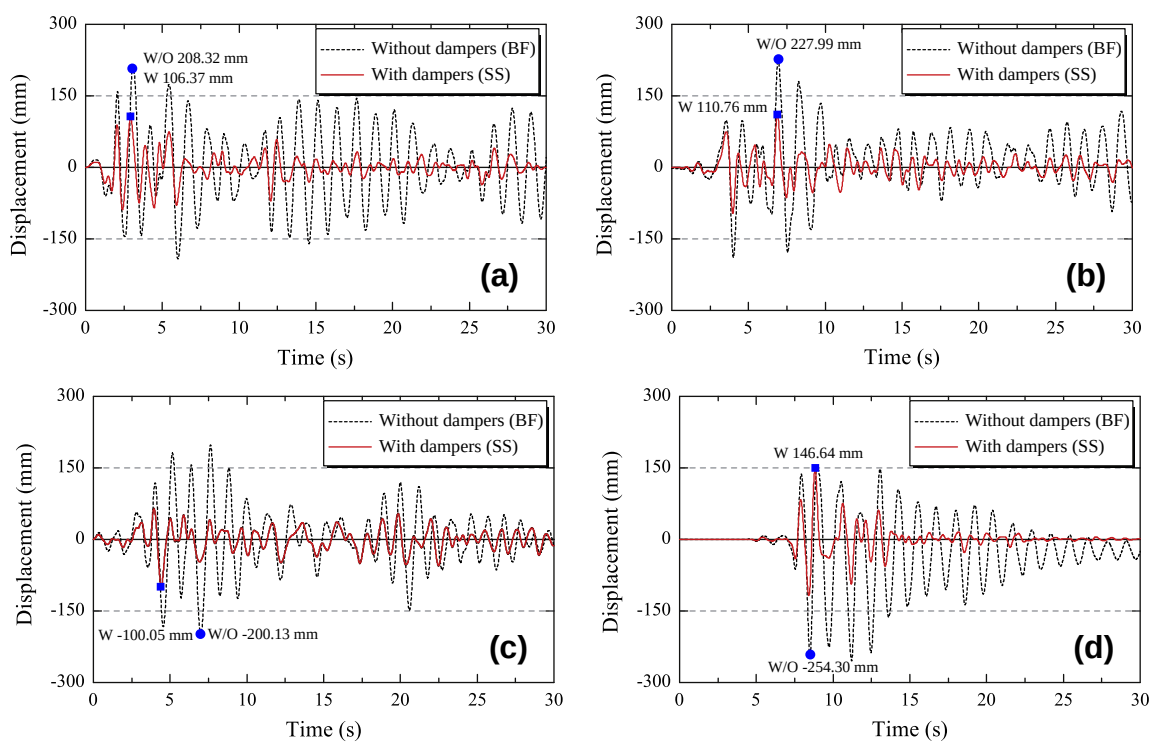

Fig. 19. Time–history response of displacement at the top floor of Model BF and SS: (a) El Centro 1940 NS, (b) Taft 1952 EW, (c) Hachinohe 1968 NS, and (d) Kobe 1995 NS.

4.4.4. Comparisons of base shear force and peak acceleration

Fig. 12a shows the maximum base shear force of each model under four earthquakes. It can be seen that the base shears of the frames with linear FVD (Model DG, CV, and SS) are smaller than that of the bare frame. The base shear of Model SS is the smallest among all models. Fig. 12b portrays peak acceleration for each model under four earthquakes. The peak accelerations of Model SS are the smallest in all cases except TAF 50.

4.4.5. Comparisons of exact model and simplified models of SEDS

To examine the applicability of the simplified models derived in Section 3, the analysis results of the exact model as shown Fig. 8d were compared with those of simplified models, which consist of the bare frame with a spring and a dashpot connected between top floor and ground (series or parallel). Table 6 presents properties of the system used in the analysis.

Fig. 13 portrays comparisons of maximum story drift angle of the three-story structure with exact model and simplified models

Table 7
Maximum displacement of the top floor of six-story structures.

Input motion	Model	Without device (mm)	With device (mm)	Ratio
El Centro	DG	208.32	178.13	0.86
	CV		155.56	0.75
	SS		106.37	0.51
Taft	DG	227.99	165.49	0.73
	CV		148.75	0.65
	SS		110.76	0.49
Hachinohe	DG	200.13	144.65	0.72
	CV		132.90	0.66
	SS		100.05	0.50
Kobe	DG	254.30	191.32	0.75
	CV		179.29	0.71
	SS		146.64	0.58

of SEDS under four ground motions presented in Table 2. The vertical axis represents the maximum story drift angles of the structures with simplified models of SEDS, and the horizontal axis signifies the maximum story drift angles of the structures with exact model of SEDS. This figure reveals that the response of the equivalent Maxwell model agrees well with that of the exact model, whereas the response of the generalized Kelvin model fluctuates within 10% of the exact model.

4.5. Seismic responses of six-story structure

4.5.1. Parameter analysis results

Fig. 14 depicts the maximum story drift angle for Model SS of the six-story structure. The values of rod stiffness k_B range from 15 kN/mm to 65 kN/mm and the values of damping coefficient C_D range from 0 kN s/mm to 10 kN s/mm. The model with a damping coefficient of zero is identical to the bare frame. Results of parameter analysis show that the maximum story drift angle is the smallest for $C_D = 2$ kN s/mm. For cases of $C_D > 2$ kN s/mm, the maximum story drift angle varies according to the rod stiffness. For the Kobe earthquake, in cases where $C_D = 10$ kN s/mm and the rod stiffness is small, the maximum story drift angle becomes very large, which reveals that the balance between the damping coefficient and rod stiffness is important in the design of the proposed system.

Fig. 15 portrays the effects of the rod stiffness and damping coefficient on the damper deformation for the El Centro and Kobe earthquakes. The damper deformation decreases as the damping coefficient decreases. The rod stiffness has little influence on the damper deformation.

Fig. 16 depicts the effects of rod stiffness and damping coefficient on the dissipated energy of FVDs for El Centro and Kobe earthquakes. When the damping coefficient range from 0 to 3 kN s/mm, the dissipated energy of FVDs increases as the damping coefficient increases. In the range of $C_D > 3$ kN s/mm, the dissipated energy decreases gradually as C_D increases. For cases where the rod stiffness is larger than 35 kN/mm, the rod stiffness has little influence on the dissipated energy of FVDs.

Fig. 17 shows the effects of rod stiffness and damping coefficient on the rod deformation for El Centro and Kobe earthquakes. The rod deformation increases as the damping coefficient increases for each value of rod stiffness. For each value of the damping coefficient, the rod deformation increases as the rod stiffness decreases.

From the parameter analysis results presented in Figs. 14–17, the value of $C_D = 2$ kN s/mm and $k_B = 35$ kN/mm are adopted for the seismic response analysis presented in the next section.

4.5.2. Seismic responses of six-story structure

Fig. 18 depicts the maximum story drift angle distributions. The maximum story drift angles of BF are larger than 0.01 rad for all earthquakes. In contrast, the maximum story drift angles of Model SS are smaller than 0.01 rad for all earthquakes. They are smallest among the models with dampers.

Fig. 19 shows time–history responses of displacement at the top floor of Model BF and Model SS. Displacement is reduced by implementing SEDS. For the Kobe earthquake, residual displacement at the final stage of analysis is reduced by the proposed system. Table 7 presents the maximum displacement of the top floor and the ratio of the value with dampers to that without dampers.

5. Conclusion

This paper presented a new vibration control system based on the seesaw mechanism with fluid viscous dampers. The proposed seesaw energy dissipation system (SEDS) comprises three parts: Brace, Seesaw, and Fluid viscous dampers (FVDs). By introducing pre-tension in rods, long steel rods are applicable as bracing and can be located over several stories as in the Model SS.

First, the simplified analysis models for SEDS were presented and evaluated. The results of dynamic response analysis reveal that the simplified analysis models are available for analysis of SDOF.

To confirm the applicability of SEDS, seismic response analyses were then conducted for three-story and six-story frames with an energy dissipation system. The diagonal-brace-FVD system and the chevron-brace-FVD system are also analyzed for comparison. The maximum story drift angle distributions, the time–history responses of displacement at the top floor, plastic hinge formation, base shear force, and peak acceleration were examined. The results of analyses demonstrated that the proposed system can reduce the seismic response of the frames effectively. Results show that the configuration method of the damping device influenced the damping effect. The analysis model in which the bracing members connect the proposed damping device at the ground level directly to the top story beams in the other bay exhibited the greatest reduction of deformation.

The parameter analyses related to the effect of rod stiffness and damping coefficient on the seismic response of the steel moment frames with SEDS using FVDs revealed that the important point in the design of this system is the balance between the damping coefficient and rod stiffness.

This paper presented the first report of an investigation into the potential of seesaw energy dissipation system with FVDs for the seismic protection of structures. The system configurations are preliminary concepts. Therefore, further experimental and analytical work is necessary to validate the results of the preliminary study.

One benefit of the proposed system is that it enables long steel rods to be used as bracing between the seesaw mechanism members and the moment frame connections over some stories.

References

[1] Constantinou MC, Tsopelas P, Hammel W, Sigaher AN. Toggle–brace–damper seismic energy dissipation systems. J Struct Eng 2001;127(2):105–12.
[2] Chen YT, Chai YH. Effects of brace stiffness on performance of structures with supplemental maxwell model-based brace-damper systems. Earthquake Eng Struct Dynam 2011;40:75–92.
[3] Marshall JD, Charney FA. Seismic response of steel frame structures with hybrid passive control systems. Earthquake Eng. Struct. Dynam. 2012;41(4):715–33.
[4] Constantinou MC, Soong TT, Dargush GF. Passive energy dissipation systems for structural design and retrofit. Buffalo (NY): Multidisciplinary Center for Earthquake Engineering Research Center; 1998.
[5] Hanson RD, Soong TT. Seismic design with supplemental energy dissipation devices. Oakland (CA): Earthquake Engineering Research Institute; 2001.
[6] Symans MD, Charney FA, Whittaker AS, Constantinou MC, Kircher CA, Johnson MW, McNamara RJ. Energy dissipation systems for seismic applications: current practice and recent developments. J Struct Eng 2008;134(1):3–21.
[7] Ibrahim YE, Marshall J, Charney FA. A visco-plastic device for seismic protection of structures. J Constr Steel Res 2007;63(11):1515–28.

[8] Tsai K, Chen H, Hong C, Su S. Design of steel triangular plate energy absorbers for seismic resistant construction. Earthq Spectra 1993;9(3):505–28.
[9] Dargush GF, Soong TT. Behavior of metallic plate dampers in seismic passive energy dissipation systems. Earthq Spectra 1995;11(4):545–68.
[10] Dimova SL, Hirata K. Simplified seismic fragility analysis of structures with two types of friction devices. Earthq Eng Struct Dynam 2000;29(8):1153–75.
[11] Gluck J, Ribakov Y. Semi-active friction damping system with amplifying braces for control of MDOF structures. Struct Des Tall Build 2001;10(2):107–20.
[12] Sabelli R, Mahin S, Chang C. Seismic demands on steel braced frame buildings with buckling-restrained braces. Eng Struct 2003;25(5):655–66.
[13] Wada A, Huang Y, Iwata M. Passive energy technology for buildings in Japan. Progr Struct Eng Mater 2000;2:335–50.
[14] Tagawa H, Gao J. Evaluation of vibration control system with U-dampers based on quasi-linear motion mechanism. J Constr Steel Res 2012;70:213–25.
[15] Kishiki S, Ohkawara Y, Yamada S, Wada A. Experimental evaluation of cyclic deformation capacity of U-shaped steel dampers for base-isolated structures. J Struct Constr Eng Trans AIJ 2008;624:333–40 [in Japanese].
[16] Zhang RH, Soong TT. Seismic design of viscoelastic dampers for structural applications. J Struct Eng 1992;118(5):1375–92.
[17] Kasai K, Fu Y, Watanabe A. Passive control systems for seismic damage mitigation. J Struct Eng 1998;124(5):501–12.
[18] Kim J, Ryu J, Chung L. Seismic performance of structures connected by viscoelastic dampers. Eng Struct 2006;28(2):183–95.
[19] Ou JP, Long X, Li QS. Seismic response analysis of structures with velocity-dependent dampers. J Constr Steel Res 2007;63(5):628–38.
[20] Kang J, Tagawa H. Seismic response analysis of steel moment frames with viscoelastic dampers based on quasi-linear motion mechanism. In: Proceedings of the eighth international conference on urban earthquake engineering (8CUEE), Tokyo; 2011 [on CD].
[21] Choi H, Kim J. New installation scheme for viscoelastic dampers using cables. Can J Civ Eng 2010;37(9):1201–11.
[22] Miyamoto HK, Gilani ASJ, Wada A, Ariyaratana C. Limit states and failure mechanisms of viscous dampers and the implications for large earthquakes. Earthq Eng Struct Dynam 2010;39(11):1279–97.
[23] Sigaher AN, Constantinou MC. Scissor–jack–damper energy dissipation system. Earthq Spectra 2003;19(1):133–58.
[24] Gluck J, Ribakov Y. Active viscous damping system with amplifying braces for control of MDOF structures. Earthq Eng Struct Dynam 2002;31(9):1735–51.
[25] Ribakov Y, Reinhorn AM. Design of amplified structural damping using optimal considerations. J Struct Eng 2003;129(10):1422–7.
[26] Lee D, Taylor DP. Viscous damper development and future trends. Struct Des Tall Build 2001;10(5):311–20.
[27] Dicleli M, Mehta A. Seismic performance of chevron braced steel frame with and without viscous fluid dampers as a function of ground motion and damper characteristics. J Constr Steel Res 2007;63(8):1102–15.
[28] Martinez-Rodrigo M, Romero ML. An optimum retrofit strategy for moment resisting frames with nonlinear viscous dampers for seismic applications. Eng Struct 2003;25(7):913–25.
[29] Kang JD, Tagawa H. Vibration control system for structures with long rods and seesaw mechanisms. In: Proceedings of the 2011 international conference on advances in structural engineering and mechanics (11'ASEM), Seoul; 2011 [on CD].
[30] Kang JD, Tagawa H. Seismic response of steel structures with seesaw systems using viscoelastic dampers. Earthq Eng Struct Dynam 2013;42(5):779–94.
[31] SNAP Technical manual. ver.5, 2009, Kozo System, Inc., Tokyo, Japan.
[32] JSSI. Design and construction manual for passively controlled buildings. 2nd ed. Japan Society of Seismic Isolation; 2005.